JOURNAL OF GEOPHYSICAL RESEARCH, VOL. 98, NO. E2, PAGES 3469–3476, FEBRUARY 25, 1993

Microcraters on Mars: Evidence for Past Climate Variations

ASHWIN R. VASAVADA, THOMAS J. MILAVEC, AND DAVID A. PAIGE

Department of Earth and Space Sciences, University of California, Los Angeles

Mars climate models predict hundredfold or greater variations in the mass of the Martian atmosphere due to large amplitude variations in Mars' obliquity through time. The production rates of impact craters on the Martian surface should be greatly affected by these atmospheric mass variations. We have constructed a simulation of the meteor bombardment of Mars which shows that during periods of the lowest theoretical atmospheric mass, the production rates of centimeter-sized hypervelocity impact craters are increased significantly. These results imply that limited in situ observations of microcraters visible on Martian rock faces could validate major aspects of the astronomical theory for climate change on Mars.

INTRODUCTION

There are several reasons to suspect that the climate of Mars has changed significantly through time. Dynamical models predict that Mars' orbital and axial elements have undergone large-scale quasi-periodic variations that have resulted in major changes in the latitudinal distribution of incident solar radiation, particularly at the poles [*Ward*, 1974*a*]. Presently, Mars has an atmosphere composed dominantly of CO_2 gas that is apparently in solid-vapor equilibrium with a small CO_2 deposit at the south residual polar cap [*Leighton and Murray*, 1966; *Kieffer*, 1979; *Fanale et al.*, 1982; *Paige et al.*, 1990]. Mars climate models predict that changes in polar insolation rates can dramatically alter the partitioning of available CO_2 between the atmosphere and residual polar CO_2 deposits [*Ward* 1974*b*; *Toon et al.*, 1980]. During periods when polar insolation rates are high, residual CO_2 polar caps may increase the atmospheric mass, or they may sublimate completely. During periods when polar insolation rates are low, residual polar caps can dramatically decrease the atmospheric mass because of their lowered vapor pressures. During periods when polar insolation rates are at their lowest, nearly all the CO_2 in the cap-atmosphere system is expected to be cold trapped onto residual polar caps, and the atmosphere may consist only of the remaining noncondensible species Ar and N_2 [*Lindner and Jakosky*, 1985].

As it presently stands, we have no definitive evidence that Mars has in fact experienced recent large-scale astronomically driven climate change. The most suggestive information obtained to date has come from orbiter images of the north and south polar regions, which show layered deposits of dust and ice that have been widely interpreted as being evidence that the rates of accumulation of these materials at the poles has varied cyclically [*Murray et al.*, 1972; *Carr*, 1982]. The depths of the thinnest layers that presently can be discerned are of the order of 30 m, but layering may also be present at depth scales beyond the resolution limits of the best available orbiter imagery. Estimating the timescales over which the observable layers have accumulated has proven difficult, but crater counts on the south polar layered deposits have yielded estimates of 0.1 km/b.y. [*Plaut et al.*, 1988]. Analysis of the size-frequency distributions and depth profiles of large impact craters elsewhere on the Martian surface has suggested that the surface of Mars has undergone periods of enhanced erosion [*Hartmann*, 1973; *Chapman*, 1974; *Barlow*, 1990]. Whether these erosional epochs are linked to astronomically forced climate change is presently not clear.

It has occurred to us that the Martian cratering record for size ranges smaller than have yet been observed also may be a partial record of astronomically driven climate variations. The Martian atmosphere in its present condition prevents the formation of small hypervelocity impact craters on the Martian surface. However, during periods when polar insolation rates are small, the Martian atmosphere may no longer be massive enough to prevent these impacts. If the periods of low atmospheric mass are long enough to allow a significant number of small impact craters to accumulate, then observations of these craters could validate major aspects of the astronomical theory for climate change on Mars.

In the following sections, we explore this possibility quantitatively. First, we review the effects of atmospheric drag and ablation on incident meteors, and we present calculations of surface impact velocities and resulting crater diameters over a range of initial meteoroid diameters and atmospheric masses. We then present the results of a Monte Carlo calculation in which we simulate the bombardment of the surface of Mars through time using estimates of the incident meteoroid flux and the variation of Mars' obliquity and atmospheric mass. In the final section, we discuss our results, their potential uncertainties, and the prospects of observing the Martian microcrater record.

ATMOSPHERIC EFFECTS ON IMPACT CRATERING

Interaction With the Atmosphere

The forces on a meteor due to aerodynamic drag and Mars' gravity are

$$\frac{dv}{dt} = \frac{-C_D \rho_{atm} A v^2}{2m} + g\cos\theta \qquad (1)$$

where ρ_{atm} is the local density of the atmosphere; A, v, and

Paper number 92JE02942.
0148-0227/93/92JE-02942$05.00

m are the cross-sectional area, velocity, and mass of the meteor; and g is the local gravitational acceleration. It is assumed that the meteors are spherical and that their density is 3.4 g cm^{-3}. The angle of the meteor's trajectory with the surface normal varies according to *Melosh* [1989] as

$$\frac{d\theta}{dt} = \frac{g\sin\theta}{v} \tag{2}$$

Many previous studies of meteoroid ablation [*Flynn*, 1989; *Ip*, 1990] needed only to model the forces acting on a meteor in the regions of the atmosphere where ablation takes place. Because in this study we model a meteor's entire journey to the surface, it becomes necessary to account for all regions of the atmosphere and thus all flow conditions. The mean free path of an atmospheric gas molecule decreases with altitude, becoming small when compared to the size of a meteor. As this happens, the flow regime around the meteor changes from free-molecular to continuum flow and the value of the drag coefficient, C_D decreases [*Masson et al.*, 1960]. In order to model the aerodynamic drag on planetesimals in protoplanetary atmospheres, *Podolak et al.* [1988] used an empirical relation between the Reynolds number of a flow around a sphere and the measured drag on that sphere. The value of the drag coefficient is dependent upon the sphere's size and speed and the atmosphere's constituency, density, and viscosity. According to their work, the Reynolds number of the flow around a spherical particle Re is defined as

$$Re = \frac{\rho_{atm} v r}{\eta} \tag{3}$$

where v and r are the particle's velocity and radius and η is the atmosphere's viscosity. The atmosphere's viscosity

$$\eta = \mu \frac{\langle v_g \rangle}{3\sqrt{2}\pi d^2} \tag{4}$$

is dependent on the mean molecular speed of the gas molecules,

$$\langle v_g \rangle = \sqrt{\frac{8kT}{\pi\mu}} \tag{5}$$

where k is Boltzmann's constant, T is the ambient gas temperature, μ is the mass of a gas molecule, and d is the diameter of a gas molecule, taken to be that of CO_2, 4.5× 10^{-10} m. Matching the empirical data, *Podolak et al.* then defined the drag coefficient C_D to be 2.2 if $Re < 1$, 2.2-log(Re)/3 if $1 < Re < 10^3$, and 1.0 if $Re > 10^3$.

Part of the kinetic energy of the impinging atmospheric gas molecules goes into heating the meteor and sublimating its surface, while the balance is thermally radiated away. The total energy balance for a meteor in flight through an atmosphere can be written as

$$\Lambda \tfrac{1}{2} A \rho_{atm} v^3 = 4A\varepsilon\sigma\left(T_m^4 - T^4\right) + mC\frac{dT_m}{dt} - L\frac{dm}{dt} \tag{6}$$

The fraction of the kinetic energy of the gas molecules which is transferred to the meteor, Λ, is taken to be 0.2 [*Ip*, 1990; *Bronshten*, 1983]. T_m, m, C, and L are the temperature, mass, specific heat, and heat of vaporization of the meteor, and T is the ambient gas temperature (the temperature of the atmosphere). The emissivity, ε, of the meteor is assumed to be unity, and σ is the Stephan-Boltzmann constant. The initial temperature of the meteoroid is taken to be 320 K (a blackbody at 1.52 AU) and the time step of the simulation is chosen to be 0.05 s if the temperature of the meteor is above 320 K, otherwise 0.1 s. We also assume that the entire particle comes to the temperature of the surface before the next time step. The rate of mass ablation by vaporization is then (in cgs)

$$\frac{dr}{dt} = \frac{P_v}{\rho_m \langle v_m \rangle} \tag{7}$$

The mean molecular velocity of the meteoritic material is (in cgs)

$$\langle v_m \rangle = \sqrt{\frac{8kTN_A}{\pi\nu}} \tag{8}$$

Here P_v, ρ_m, and ν are the vapor pressure, density, and molecular mass of the meteoritic material and N_A is Avagadro's number. We used following physical parameters from *Podolak et al.* [1988] to describe "rocky" meteors: C = 895 J kg^{-1} K^{-1}, L = 8.1×10^6 J kg^{-1}, $\log_{10}P_v$ = -24,605/T_m+13.176, and ν = 50 g mol^{-1}. The barometric equation gives the atmospheric density as a function of altitude, z, $\rho_{atm} = \rho_s e^{-z/H}$, where ρ_s is the atmospheric density at the surface, and H is the scale height, calculated from $H = RT/m_{atm}g$, where R is the universal gas constant and m_{atm} is the mean molecular mass of the atmospheric constituents. The temperature of the Martian atmosphere, T, is assumed to be constant with height and obliquity and is taken to be 155 K in order to be representative of the temperature and scale height profiles made during entry by the Viking landers [*Seiff and Kirk*, 1977] for heights above about 30 km. Atmospheric density is related to the atmospheric pressure at the surface through the ideal gas law. We chose to study the atmospheric effects on impact cratering with four model atmospheres ranging from the atmosphere expected at the lowest obliquity to the current atmosphere. At lowest obliquity, only the noncondensible species remain and the atmospheric surface pressure is 0.244 mbar [*Lindner and Jakosky*, 1985]. The other cases assume progressively more CO_2 gas, with total surface pressures of 0.5, 2, and 6 mbar.

Cratering Processes

We use an energy-crater diameter relation based on experimental results by *Gault* [1973] in order to scale hypervelocity impacts (all in cgs),

$$D = 10^{-2.823} \times \rho_m^{1/6} \times \rho_T^{-1/2} \times \left(\tfrac{1}{2} m v^2\right)^{0.37} \times (\cos\theta)^{0.86} \tag{9}$$

where D is the resulting hypervelocity crater diameter (in cm), ρ_m is the projectile density, and ρ_T is the target density which is assumed to be 2.8 g cm^{-3}, which would be appropriate for crystalline rocks. Our criterion for hypervelocity impacts is a constraint that the dynamic pressure of the impacting meteor must exceed the compressive strength of the impacted rock. Shock features which may identify hypervelocity impacts are expected at pressures greater than 5 GPa [*Tauber and Kirk*, 1976]. This corresponds to an impact velocity of about 1.1 km/s.

Results

We are now able to compare the effects of different atmospheric conditions on meteor survival and impact. Figures 1*a* and 1*b* show impact velocity and percentage of initial meteor mass remaining (unablated) as functions of

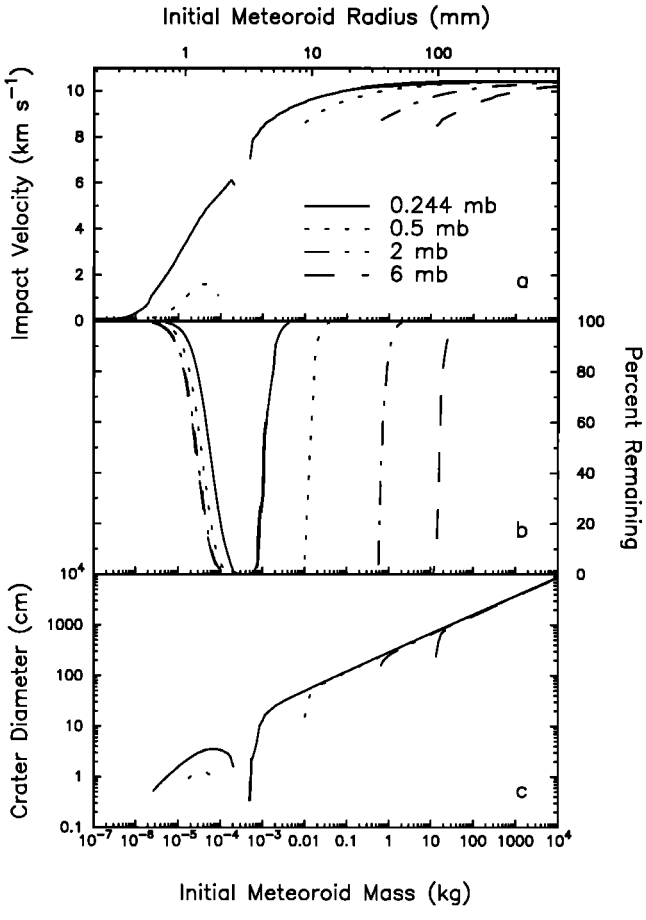

Fig. 1. Impact velocity, percentage of mass remaining (unablated), and resulting hypervelocity crater diameter for meteors entering a range of atmospheres from the atmosphere expected at low obliquity when all the CO_2 has frozen onto the poles, and the present 6-mbar Martian atmosphere. (*a*) Velocity of meteors just before impact with the surface. (*b*) Percentage of original meteoroid mass unablated during its flight through the atmosphere. (*c*) Resulting hypervelocity crater diameter, unless the meteor was completely ablated or decelerated below the hypervelocity criterion of 1.1 km/s.

initial mass for the four model atmospheric surface pressure cases. An entry velocity of 10 km/s and an entry angle of 22.5° from normal were used, both typical of Mars meteors. Figure 1*c* shows the resulting crater diameters in centimeters for those meteors that both survived the flight through the atmosphere and impacted the surface at hypervelocity. For all atmospheres there is a range of meteoroid masses for which ablation, not deceleration, is the main barrier to crater formation. For the present 6-mbar atmosphere, all meteoroids between 10^{-4} and 10 kg are completely ablated. Only meteors with initial masses above 10 kg create hypervelocity impacts; surviving meteoroids with masses below 10^{-4} kg are slowed to their terminal velocities, all below the hypervelocity criterion. Likewise for the 2-mbar case, only meteoroids with masses higher than the region affected by ablation retain enough energy to create hypervelocity impacts. For the 0.5-mbar and the 0.244-mbar atmospheres, however, meteors with masses below the completely ablated range impact the surface partially ablated but with velocities still above the hypervelocity criterion. In particular for the 0.244-mbar case, meteoroids with masses between 2×10^{-6} kg and 2×10^{-4}kg (about 0.5 to 2 mm radius) survive the flight through the atmosphere and create impact craters. The smallest crater diameter in this case is about 4 mm, 3 orders of magnitude smaller than for the case of the 6-mbar atmosphere, where the smallest possible crater size is approximately 3 m. Decreasing the atmospheric mass on Mars, then, allows the production of impact craters which are unable to be formed under the current 6-mbar atmosphere.

MONTE CARLO SIMULATION

In order to judge the significance of the effects of atmospheric mass variations through time on the cratering record, we have constructed a Monte Carlo model which simulates the meteoroid bombardment of the surface of Mars over the last 10 m.y. The model requires the quantitative specification of the flux of meteoroids in the vicinity of the planet and the variation of the atmospheric mass through time.

Meteoroid Flux Parameters

Most of our knowledge of the parameters of the subcentimeter meteoroid flux (the size range relevant to this study) has come from the study of lunar rocks and from experiments on Earth-orbiting satellites and interplanetary space probes. The absence of an atmosphere on the Moon allows the full mass range of meteors to impact the lunar surface. A comprehensive laboratory study of lunar microcraters was made possible by the return of rock samples during the Apollo era. Population densities and cratering mechanisms were studied, and absolute crater ages and production rates were determined by studies of solar flare tracks [*Hartung et al.*, 1973]. Figure 2 shows lunar rock 14312 with several microcraters or "zap pits". Experiments on Earth-orbiting satellites have yielded estimates of the distributions of meteoroid mass, direction, and velocity. *Grün et al.* [1985] have constructed an absolute cumulative mass-flux distribution at 1 AU based on satellite data for meteoroids between 10^{-21} kg and 10^{-1} kg which we approximately fit in the region $m > 10^{-11}$ kg with

$$F = 10^{-18.5} m^{-1.3} \quad (10)$$

where F is the cumulative flux per square meter of meteoroids with masses greater than m. Pioneer 10 measurements of the intensity of zodiacal light in the ecliptic plane indicate that the spatial density of these meteoroids probably decreases with radial distance r from the Sun as $r^{-1.5}$ [*Hanner et al.*, 1976]. The mass-flux distribution of Grün et al. was therefore scaled to Mars at 1.52 AU by multiplying by 0.53. An isotropic directional distribution is assumed in interplanetary space, which results in a distribution of incident angles at the top of the atmosphere proportional to $\sin 2\theta$ when measured from the frame of a moving planet. *Zook* [1975] presents several independently derived velocity distributions of meteoroids of equal masses entering Earth's atmosphere. We chose the curve of *Kessler* [1969] constructed from photographic observations and followed the procedure described by *Morgan et al.* [1988] to derive a theoretical velocity distribution for meteoroids near Mars. A function which approximates Kessler's near-Earth velocity distribution is first transformed to take out Earth's

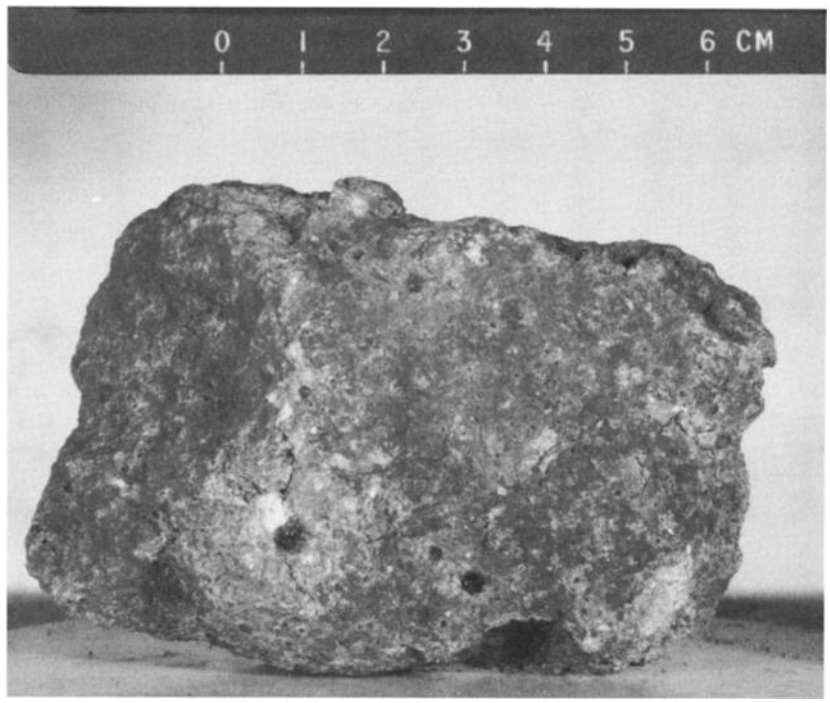

Fig. 2. Lunar rock 14312 with several microcraters or "zap pits". The largest impact chipped rock fragments to form a spall of 1 cm surrounding the 3-mm glass-lined central pit [NASA photo 2-71-31201].

gravitational focusing. Conservation of angular momentum and of meteors requires that the flux of meteors of a certain velocity near Earth be increased over the flux far from Earth's influence (but still at 1 AU) by a factor of $(v_E/v)^2$, where v_E is the velocity near Earth, and v is the velocity without gravitational focusing [*Opik*, 1951]. In addition, conservation of energy gives

$$v_E^2 = v^2 + v_{esc}^2 \tag{11}$$

where v_{esc} is the escape velocity of Earth. We find that the flux of meteors as a function of velocity excluding all gravitational effects is related to the flux of meteors near Earth by

$$f(v) = k_1\left(\frac{v}{v_E}\right)^3 f_E(v_E) \tag{12}$$

where $f(v)$ is the flux in interplanetary space at 1 AU, $f_E(v_E)$ is the flux near Earth, and k_1 is a constant needed to normalize the curve. The velocity of a meteor at a distance r from the Sun is related to the velocity of a meteor at 1 AU by $v_r = r^{-0.5}v$. If in addition it is assumed that the interplanetary velocity-flux distribution has the same shape at any distance from the Sun, then $f_r(v_r) = r^{0.5}f(v)$. Finally, Mars' gravitational influence transforms this flux distribution such that

$$f_M(v_M) = k_2 r^2\left(\frac{v_M}{v}\right)^3 f(v) \tag{13}$$

where f_M is the flux near Mars, k_2 is a normalization constant, r is 1.52 AU, and v_M is a velocity near Mars such that

$$v_M^2 = v^2 + v_{Mesc}^2 \tag{14}$$

where v_{Mesc} is Mars' escape velocity.

Atmospheric Mass Variations Through Time

Although all Mars' orbital parameters can affect polar insolation rates and thus the mass of the atmosphere, the parameter that has the largest theoretical effect is the obliquity. The exact obliquity history of Mars is presently unknown due to uncertainty in Mars' axial precession rate [*Bills*, 1990]. We chose one of several potential histories that Bills has calculated as representative of the range of obliquities Mars may have experienced. Figure 3*a* shows this obliquity history for the past 10 m.y. To construct a potential history of the mass of the Martian atmosphere, we have used this obliquity history in conjunction with a simple climate model like that first employed by *Ward* [1974*b*]. In this model, surface CO_2 partial pressures are determined by the vapor pressure of a residual solid CO_2 deposit, which is assumed to exist at one or both of the Martian poles at all times. The temperature of the solid CO_2 deposit is determined by equating the annually averaged rate of absorption of incident solar radiation at the pole with the annually averaged rate of thermal emission due to blackbody emission. Latitudinal heat transport is not considered. We assume a constant frost reflectivity of 0.667 and a constant infrared emissivity of unity. The atmosphere is also assumed to contain 0.163 mbar of nitrogen and 0.081 mbar of argon, both of which are present at all times. As can be seen in Figure 3*b*, the model gives a large variation in calculated surface pressures, which oscillate between a maximum of 52 mbar, and a minimum of 0.244 mbar when only the noncondensibles remain.

Results

The Monte Carlo simulation was run simulating the meteoritic bombardment of a 10 m^2 area of the Martian surface for 10 m.y. Incident meteors were assumed to be randomly distributed according to the angle, velocity, and mass distributions described above, but the mass of the Martian atmosphere was assumed to vary according to Figure

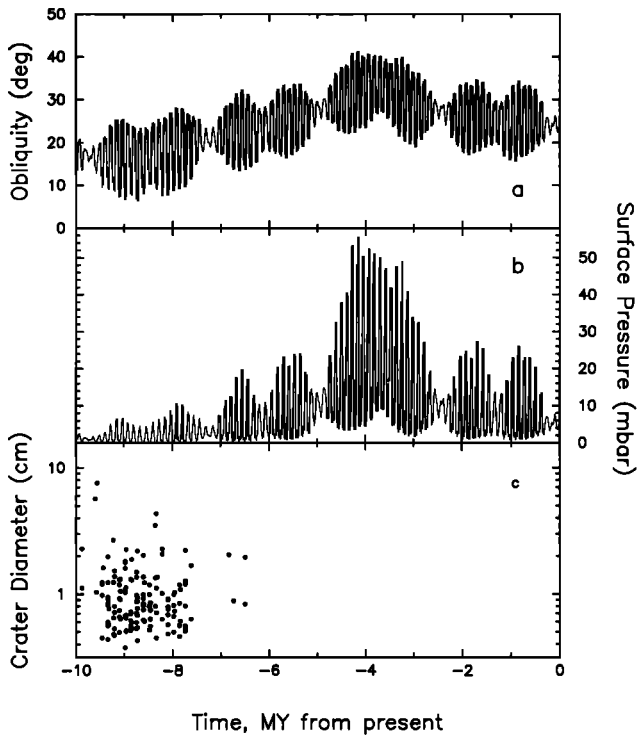

Fig. 3. (*a*) A potential Martian obliquity history from 10 m.y. ago to the present as calculated by *Bills* [1990] assuming an axial precession rate of 8.00 arc sec yr^{-1}. (*b*) A potential surface pressure history as calculated by a simple Mars climate model using the above obliquity history. (*c*) Hypervelocity impacts recorded in our simulation of a 10 m^2 surface during a 10 m.y. period with the above climate variations. Most hypervelocity impacts occurred during periods of lowest obliquity.

3*b*, with a time resolution of 20,000 years. In this period, 33,348 meteors with masses between 10^{-6} and 4.9×10^{-3} kg were incident with the atmosphere overlying the surface. Of these, 148 retained enough energy to create hypervelocity craters by the time they impacted the surface. Figures 4*a*-4*c* show histograms of the incident masses, angles, and velocities at the top of the atmosphere for all meteors considered and for those meteors that ultimately impacted the surface at hypervelocity. Figures 5*a*-5*c* show histograms of the impact masses, angles, and velocities for all meteors considered, and for those meteors that impacted the surface at hypervelocity. Figure 3*c* shows the diameters of the resulting hypervelocity impact craters as a function of time. Figure 6 shows the simulated appearance of the 10 m^2 surface after 10 m.y. Figures 7*a* and 7*b* show the resulting differential and cumulative crater size frequency distributions for the hypervelocity impact craters formed. Figure 8 shows the diameters of the hypervelocity impact craters as a function of surface pressure.

The results show that almost all of the hypervelocity craters were formed during periods of low obliquity (Figure 3*c*) and low atmospheric pressure (Figure 8). The incident meteors that were most likely to impact the surface at hypervelocity had high masses (Figure 4*c*) and lower angles of incidence (Figure 4*a*). The incident velocities of the meteors was of less importance (Figure 4*b*). Most of the meteors that did impact the surface were decelerated to some degree by the atmosphere (Figures 4*b* and 5*b*). The slope of the resulting cumulative hypervelocity crater size-frequency

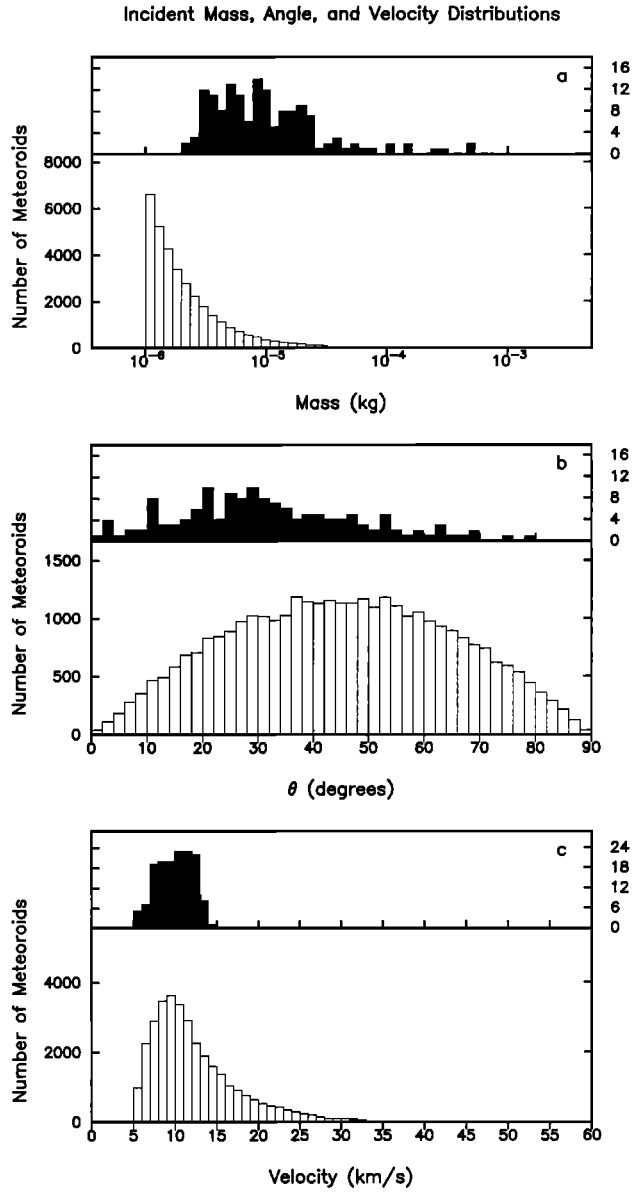

Fig. 4. Mass, angle, and velocity distributions for meteors when incident at the top of the Martian atmosphere. The outlined histograms show the distributions for all meteors. The solid histograms show the distributions for only those meteors which eventually impacted the surface at hypervelocity. (*a*) Mass distribution of meteors when incident at the top of the Martian atmosphere. (*b*) Angle distribution of meteors when incident at the top of the Martian atmosphere, measured from the normal to the surface. (*c*) Velocity distribution of meteors when incident at the top of the Martian atmosphere.

distribution is approximately -2 (Figure 7*b*). On a planet without an atmosphere, the cumulative size frequency distribution would have had a slope of approximately -3 for the population of impacting bodies considered in our simulation.

DISCUSSION

The results of our simulation indicate that the existence of small hypervelocity impact craters on Martian rocks should be a good indicator as to whether Mars has experienced prolonged periods of low atmospheric pressure. If so, the

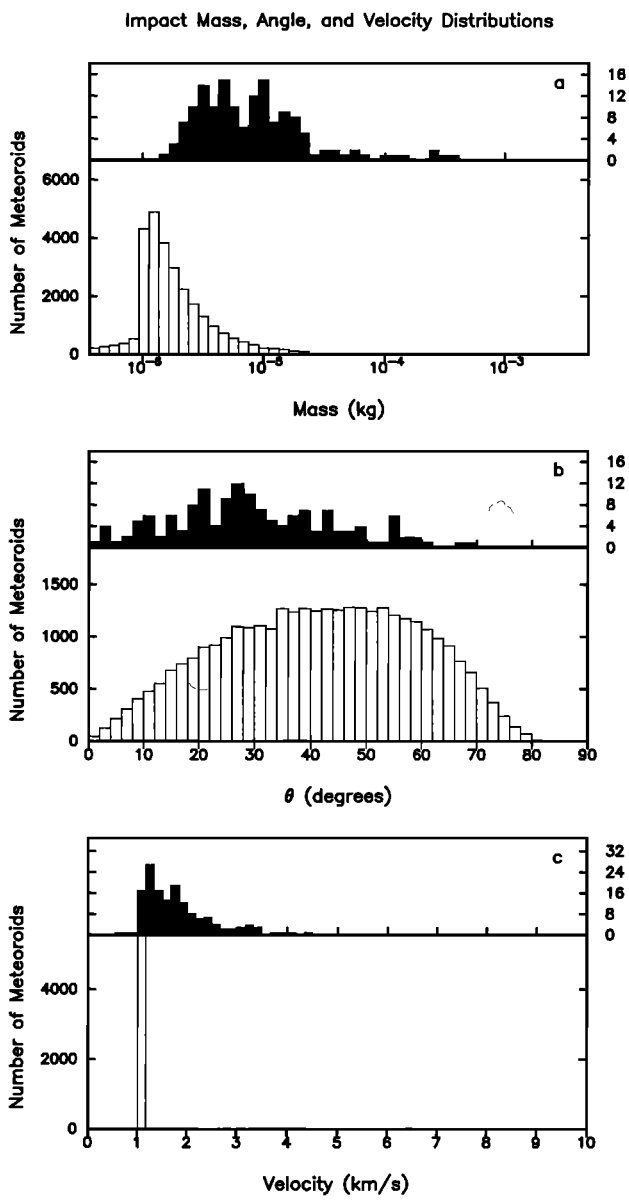

Fig. 5. Mass, angle, and velocity distributions for meteors just before impact with the Martian surface. The outlined histograms show the distributions for all meteors. The solid histograms show the distributions for only those meteors which impacted the surface at hypervelocity. (*a*) Mass distribution of meteors just before impact with the Martian surface. (*b*) Angle distribution of meteors just before impact with the Martian surface. (*c*) Velocity distribution of meteors just before impact with the Martian surface.

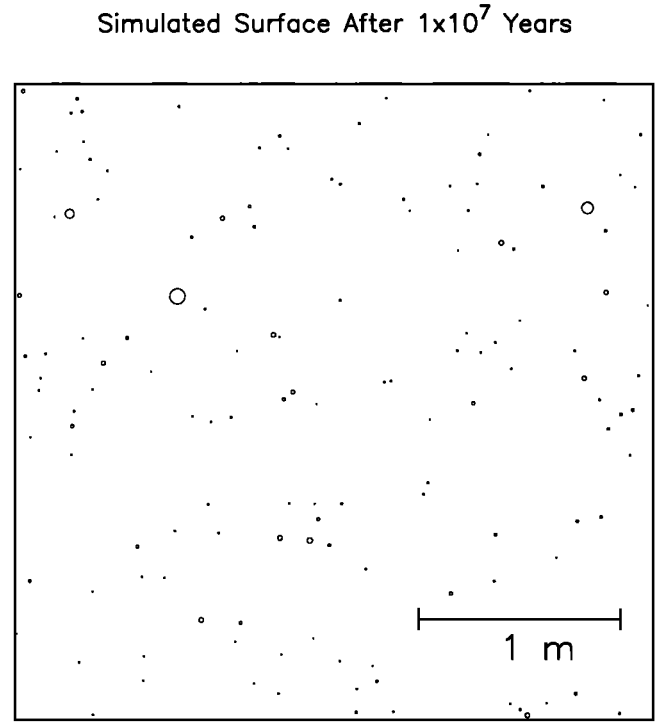

Fig. 6. Simulated hypervelocity impacts recorded on a 10 m^2 Martian surface after a 10 m.y. period experiencing the climate variations shown in Figure 3. The diameters of the circles are scaled to the diameters of the hypervelocity impact craters.

lengths and magnitudes of these periods would be reflected in the quantity and smallest sizes of hypervelocity craters seen on the surface. Conversely, if cyclic climatic change has not occurred and the current conditions have prevailed far into the past, we would not expect to see any centimeter-sized craters.

There are several uncertainties in our methods and unknown factors which may affect the validity of our results. First, the aspect of our model whose uncertainty has the most quantitative influence on the results is the absolute size-flux distribution of meteors near Mars. Obviously, variations of these rates would have proportional variations in the production rates of certain size craters on the surface, but these variations would not diminish our main conclusion, as regardless of the absolute flux, production rates of smaller craters are greatly enhanced during periods of low obliquity. Second, our model for mass variations of the Martian atmosphere through time is extremely simple. We assumed an unlimited supply of solid CO_2 at the poles and constant CO_2 frost albedos and emissivities through time. It is not known whether either of these assumptions is correct, especially during periods of high obliquity. During periods of low obliquity, however, our model is likely to be fairly realistic. This is fortunate, because these periods are of primary importance to our results. Third, considering the long time span required for significant cratering in these size ranges to occur, erosion rates must also be taken into consideration. *Arvidson et al.* [1979] have determined that little breakdown or removal of large rock features has occurred over the past millions of years, while a rapid, seasonal redistribution of loose, fine-grained material has occurred. It is also likely that erosion and deposition rates on Mars have varied spatially and temporally. We believe that microcrater populations should be best preserved and studied on rock faces such as exposed bedrock and large boulders such as those abundant at the Viking lander sites. If some rock faces have remained exposed and undisturbed for eons under an atmosphere which has experienced significant mass variation as in our model, we would expect to find saturated crater populations on their surfaces. If our results are taken at face value, then hypervelocity meteorite impacts may be a significant agent for rock breakdown on Mars. Fourth, surface elevation may also influence observations of microcrater populations. In our model, the hypothetical surface was assumed to be at the Mars reference aeroid. Surfaces at higher elevations should experience

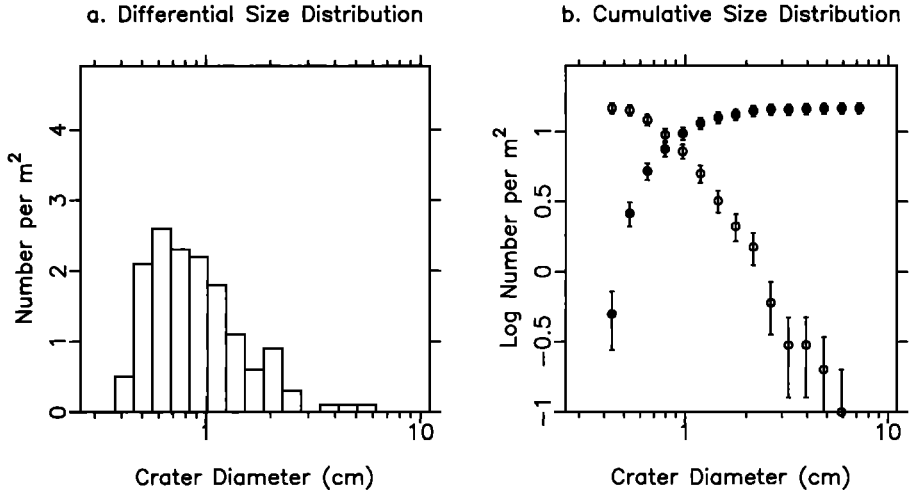

Fig 7. (*a*) Differential size distribution for hypervelocity impacts as recorded in our simulation. (*b*) Cumulative size distribution for hypervelocity impacts as recorded in our simulation, counted from both ends of the size scale.

enhanced cratering due to the shorter flight time of meteors through the thinner atmosphere. Finally, Martian rock faces may also contain secondary microcraters caused by ejecta from larger impacts. *Hörz et al.* [1971] have concluded that most secondary impacts on lunar rocks do not have sufficient impact energies to produce shock features associated with primary hypervelocity impacts. Although the energies of secondary impacts on Mars could potentially be higher than those on the Moon due to Mars' higher escape velocity, our model implies that the effects of atmospheric drag should make hypervelocity impacts by secondary particles common only during periods of low obliquity. Furthermore, shock features such as glass-lined pits within the microcraters may contain mineralogical clues as to whether or not the impacting body was meteoritic [*Hörz et al.*, 1971].

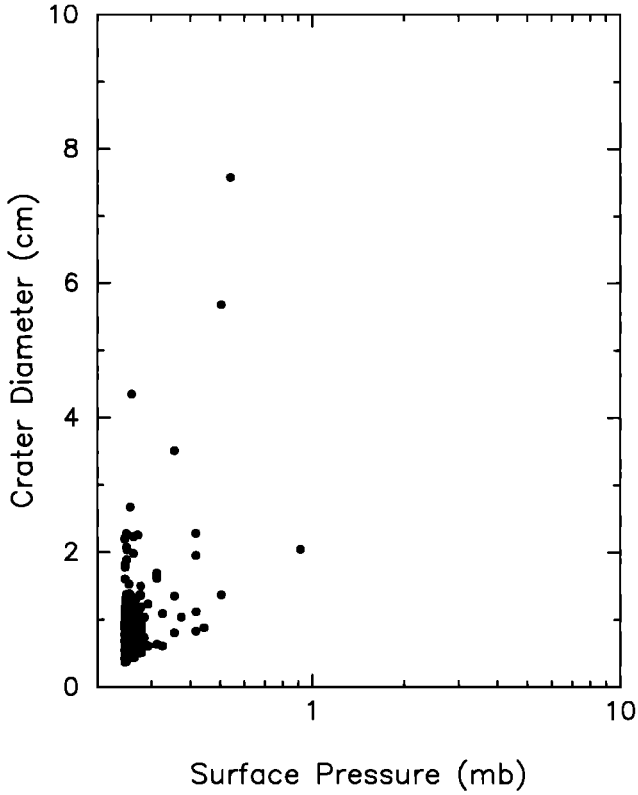

Fig. 8. Crater diameters and atmospheric surface pressures at the time of impact for the hypervelocity impacts recorded in our simulation.

In the future, studies of microcraters on the Martian surface could be accomplished by returning promising rock samples or by in situ analysis by robotic devices. Because these microcraters are expected to be best preserved on rock faces, robotic devices would be greatly facilitated by the ability to locate boulders on the surface and examine their surfaces in microscopic detail. These tasks may not necessarily require specialized dedicated instrumentation. There is also a distinct possibility that "fossil" Martian microcraters could presently lie buried in depositional environments. Studies of such deposits could extend our record of Mars' atmospheric history far into the past. The presence of microcraters anywhere on the planet would be definitive evidence that periods of significantly reduced atmospheric mass have occurred, the most probable cause of which is astronomically induced climate change. The absence of microcraters, on the other hand, would not reveal much, considering the uncertainties in microcrater production and erosion rates.

Acknowledgments. We would like to thank Bruce Bills for providing us with his computations of a Martian obliquity history, and Paul Warren for providing the photograph for Figure 2. This research was supported by the NASA Mars Surface and Atmosphere Through Time Program, NASA grant NAGW 2226, and the NASA Planetary Geology and Geophysics Program, NASA grant NAGW 2063.

REFERENCES

Arvidson, R., E. Guinness, and S. Lee, Differential aeolian redistribution rates on Mars, *Nature*, *278*, 533, 1979.

Barlow, N. G., Constraints on early events in Martian history as derived from the cratering record, *J. Geophys Res.*, 95, 14,191-14,201, 1990.

Bills, B. G., The rigid body obliquity of Mars, *J. Geophys. Res.*, *95*, 14,137-14,153, 1990.

Bronshten, V. A., *Physics of Meteoric Phenomenon*, D. Reidel, Norwell, Mass., 1985.

Carr, M. H., Periodic Climate change on Mars: Review of evidence

and effects on distribution of volatiles, *Icarus*, *50*, 129-138, 1982.

Chapman, C. R., Cratering on Mars, 1, Cratering and obliteration history, *Icarus*, *22*, 272-291, 1974.

Fanale, F. P., J. R. Salvail, W. B. Banerdt, and R. S. Saunders, Mars: The regolith-atmosphere-cap system and climate change, *Icarus*, *50*, 381-407, 1982.

Flynn, G. J., Atmospheric entry heating of micrometeorites, *Lunar Planet. Sci.*, *XIX*, 673-682, 1989.

Gault, D. E., Displaced mass, depth, diameter, and effects of oblique trajectories for impact craters formed in dense crystalline rocks, *Moon*, *6*, 32-44, 1973.

Grün, E., H. A. Zook, H. Fechtig, and R. H. Giese, Collisional balance of the meteoritic complex, *Icarus*, *62*, 244-272, 1985.

Hanner, M. S., J. G. Sparrow, J. L. Weinberg, and D. E. Beeson, Pioneer 10 observations of zodiacal light brightness near the ecliptic: Changes with heliocentric distance, in *Interplanetary Dust and the Zodiacal Light*, edited by H. Elsasser and H. Fechtig, pp. 29-35, Springer-Verlag, New York, 1976.

Hartmann, W. K., Martian cratering, 4, Mariner 9 initial analysis of cratering chronology, *J. Geophys. Res.*, *78*, 4096-4116, 1973.

Hartung, J. B., F. Hörz, F. K. Aitken, D. E. Gault and D. E. Brownlee, The development of microcrater populations on lunar rocks, *Proc. Lunar Sci. Conf., 4th*, 3213-3232, 1973.

Hörz, F., J. B. Hartung and D. E. Gault, Micrometeorite craters on lunar rock surfaces, *J. Geophys. Res.*, *76*, 5770-5798, 1971.

Ip, W.-H., Meteoroid ablation processes in Titan's atmosphere, *Nature*, *345*, 511-512, 1990.

Kessler, D. J., Average relative velocity of sporadic meteoroids in interplanetary space, *AIAA J.*, *7*, 2337-2338, 1969.

Kieffer, H. H., Mars south polar spring and summer temperatures: A residual CO_2 frost, *J. Geophys. Res.*, *84*, 8263-88, 1979.

Leighton, R. B., and B. C. Murray, Behavior of carbon dioxide and other volatiles on Mars, *Science*, *153*, 136-144, 1966.

Lindner, B. L., and B. M. Jakosky, Martian atmospheric photochemistry and composition during periods of low obliquity, *J. Geophys. Res.*, *90*, 3435-3440, 1985.

Masson, D. J., D. N. Morris, and D. E. Bloxsom, Measurements of sphere drag from hypersonic continuum to free-molecular flow, *Rarefied Gas Dyn.*, *3*, 643-661, 1961.

Melosh, H. J., *Impact Cratering: A Geologic Process*, Oxford University Press, New York, 1989.

Morgan, T. H., H. A. Zook, and A. E. Potter, Impact-driven supply of sodium and potassium to the atmosphere of Mercury, *Icarus*, *75*, 156-170, 1988.

Murray, B. C., L. A. Solderblom, J. A. Cutts, R. P. Sharp, D. J. Milton and R. B. Leighton, Geologic framework of the south polar region of Mars, *Icarus*, *17*, 328-345, 1972.

Opik, E. J., Collision probabilities with the planets and the distribution of interplanetary matter, *Proc. R. Irish Acad., Sect. A*, *54*, 165-199, 1951.

Paige, D. A., K. E. Herkenhoff, and B. C. Murray, Mariner 9 observations of the south polar cap of Mars: Evidence for residual CO_2 frost, *J. Geophys. Res.*, 95, 1319-35, 1990.

Plaut, J. J., R. Kahn, E. A. Guiness, and R. E. Arvidson, Accumulation of sedimentary debris in the south polar region of Mars and implications for climate history, *Icarus*, *76*, 357-77, 1988.

Podolak, M., J. B. Pollack, and R. T. Reynolds, Interactions of planetesimals with protoplanetary atmospheres, *Icarus*, *73*, 163-179, 1988.

Seiff, A., and D. B. Kirk, Structure of the atmosphere of Mars in summer at mid-latitudes, *J. Geophys. Res.*, *82*, 4364-4378, 1977.

Tauber, M. E., and D. B. Kirk, Impact craters on Venus, *Icarus*, *28*, 351-357, 1976.

Toon, O. B., J. B. Pollack, W. Ward, J. A. Burns and K. Bilski, The astronomical theory of climactic change on Mars, *Icarus*, *44*, 552-607, 1980.

Ward, W. R., Climatic variations on Mars, 1, Astronomical theory of insolation, *J. Geophys. Res.*, *79*, 3375-3386, 1974*a*.

Ward, W. R., Climatic variations on Mars, 2, Evolution of carbon dioxide atmosphere and polar caps, *J. Geophys. Res.*, *79*, 3387-3395, 1974*b*.

Zook, H. A., The state of meteoritic material on the Moon, *Proc. Lunar Sci. Conf., 6th*, 1653-1672, 1975.

T. J. Milavec, D. A. Paige, and A.R. Vasavada, Department of Earth and Space Sciences, University of California, Los Angeles, CA 90024.

(Received January 27, 1992;
revised December 15, 1992;
accepted December 15, 1992.)